IOPscience iopscience.iop.org

Home Search Collections Journals About Contact us My IOPscience

Resistance behaviour and morphological changes during electromigration in gold wires

This article has been downloaded from IOPscience. Please scroll down to see the full text article.

2007 J. Phys.: Condens. Matter 19 046210

(http://iopscience.iop.org/0953-8984/19/4/046210)

View the table of contents for this issue, or go to the journal homepage for more

Download details:
IP Address: 129.252.86.83
The article was downloaded on 28/05/2010 at 15:56

Please note that terms and conditions apply.

INSTITUTE OF PHYSICS PUBLISHING JOURNAL OF PHYSICS: CONDENSED MATTER
J. Phys.: Condens. Matter **19** (2007) 046210 (11pp) doi:10.1088/0953-8984/19/4/046210

Resistance behaviour and morphological changes during electromigration in gold wires

B Stahlmecke and G Dumpich

Fachbereich Physik, Universität Duisburg-Essen, Lotharstraße 1, 47057 Duisburg, Germany

E-mail: burkhard.stahlmecke@uni-due.de

Received 4 October 2006, in final form 19 December 2006
Published 12 January 2007
Online at stacks.iop.org/JPhysCM/19/046210

Abstract
We present *in situ* scanning electron microscope electromigration measurements on fine-grained gold nanowires. The grain size of 20–40 nm is much smaller than the wire width of $\simeq 1$ μm. Electrical breakdown occurs in a slit-like manner, which has been observed commonly for bamboo-like or single-crystalline wires. Furthermore, the development of void area is determined and found to increase linearly over time for these polycrystalline wires. Also, the local enhancement of the current density at the position of the critical voids is determined. In addition, calculations of the temperature increase at the position of electrical breakdown reveal a locally reduced energy dissipation belonging to the position with the highest current density.

1. Introduction

Electromigration (EM) continues to be the most important reliability issue in integrated circuits. Despite the ongoing research for the past 50 years, the interplay between the different parameters influencing electromigration in metals is far from being understood completely [1]. The main focus of (industrial) research is dedicated to the prolongation of lifetime under operating conditions, since electromigration failure was identified as a serious reliability problem [2–4].

Whereas in former times aluminium was used as metallization in integrated circuits, this metal is now grossly replaced by copper metallizations [5, 6]. Using the famous Black equation [7], accelerated lifetime tests have been performed and successfully adopted to operating conditions. It was found early that the addition of small amounts of copper in aluminium and now of tin in copper [4, 8] can reduce EM damage in a wire significantly. Furthermore, the influence of the grain size on EM damage was investigated to enhance the lifetime of a metallization [9]. To ensure that EM testing is comparable between different laboratories, a standard test layout was developed to determine parameters like the activation energy for electromigration, the effective valence of the ions or the median time to failure for

0953-8984/07/046210+11$30.00 © 2007 IOP Publishing Ltd Printed in the UK

an identical set of wires. For wafer-level tests, there exists a variety of different accelerated test methods like the SWEAT method (see i.e. [10, 11]).

A great number of works are devoted to the morphological development of wires under EM conditions, either from experimental [12, 13] or from theoretical points of view [14, 15]. These studies have in common that they have concentrated in recent times mainly on large-grained, bamboo-like or even single-crystalline wires [16, 17], whereas the case of fine-grained wires (see, for instance, [18]) is not commonly taken into account.

In the study presented here, the focus is on electromigration behaviour in fine-grained material. The aim of the study is not to determine parameters like the activation energy or the effective valance for gold nanowires on silicon substrates. Rather, we would like to give new insight to typical morphological developments during electromigration in fine-grained material obtained by *in situ* scanning electron microscope (SEM) observations. Therefore, the development of void area and the breakdown dynamics will be investigated in more detail.

This paper is organized as follows. After a brief introduction of the experimental methods in section 2, the dependence of the resistance increase as a function of current will be discussed in section 3.1. In section 3.2 the development of voids and hillocks of a typical *in situ* SEM electromigration experiment on polycrystalline gold wires will be described and discussed. The resistance behaviour of this wire is presented in section 3.3, followed by a detailed analysis of the breakdown position in section 3.4.

2. Experimental setup and sample preparation

Gold wires are prepared using a standard two-step electron-beam lithography process and subsequent thermal evaporation of gold under high vacuum conditions ($p \sim 5 \times 10^{-6}$ mbar) on silicon substrates ($\rho \simeq 1\ \Omega$ cm) covered with native oxide [19]. The wires have typical dimensions of length $l \simeq 10\ \mu$m, width $w \simeq 1\ \mu$m and thickness $t \simeq 36$ nm. The length and width of the wires are determined from SEM images; the thickness is determined using a calibrated thermal evaporation system and is subsequently controlled by atomic force microscopy (AFM). Electrical contact to the nanowires is established by a standard bonding technique to attach aluminium wires from a 16-pin chip carrier to macroscopic bond pads. The pads are connected to the nanowires in a four-point geometry. The *as-prepared* wires, without applying any current, have a lognormally distributed median grain size of approximately 27 nm, as determined according to SEM images and confirmed by transmission electron microscope investigations.

The electromigration measurements are conducted inside a LEO 1530 SEM at a pressure below 3×10^{-6} mbar. The measurements are performed at room temperature using the constant-voltage mode of a Keithley 2400 Source-Measure-Unit. The current density at the beginning of the experiment has a value above 1×10^{8} A cm^{-2}, which is necessary to conduct the measurements within a reasonable time interval[1]. The morphological changes (that is, the formation of voids and hillocks) taking place in the wire are observed in real time using the video capability of the SEM: an audio visual interleave-movie is recorded during the whole time of the electromigration test. This allows us to follow the morphological development of voids and hillocks within the time interval that is necessary for the SEM beam to scan one frame (i.e. for the measurements presented here, a time interval of approximately $\Delta t = 10$ s). Single images can be extracted at defined times from this movie to determine the area of voids and,

[1] Due to contaminations taking place during the *in situ* SEM experiments, a reasonable time for such a study is of the order of about 10 h. These contaminations might prevent grain growth, as will be presented in a forthcoming publication [20]. Furthermore, the electron beam might lead to periodic resistance oscillations [21]. These effects can be neglected in the present study.

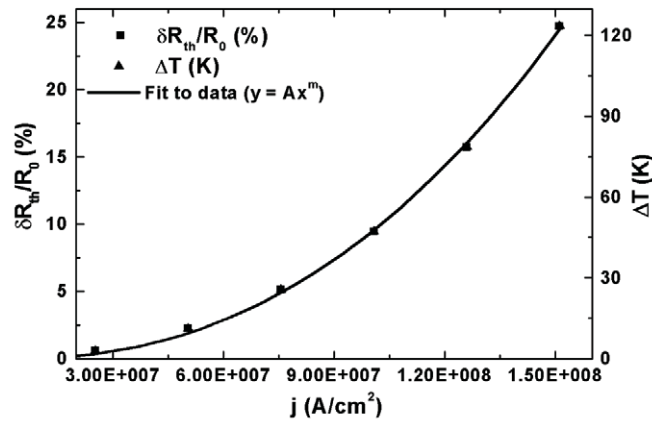

Figure 1. Relative resistance increase and calculated temperature increase as a function of current density for a polycrystalline gold nanowire.

in connection with the electrical data, the current density in the wire. This is done by applying standard graphic software like Adobe Photoshop using the grey-scale values within a certain interval in the vicinity of a void. The number of pixels which have similar grey-scale values is then compared with the complete number of pixels of the imaged nanowire. As a result, the ratio of the void area with respect to the overall nanowire area is determined.

3. Experimental observations and discussion

3.1. Dependence of resistance change on current density

To perform electromigration experiments it is crucial to know the temperature of the nanowire under investigation. Unfortunately, it is quite difficult to actually measure the temperature of the wire itself. Therefore an indirect method is applied using the resistance change due to the Joule heating of the wire. With a resistance change δR_{th}, the temperature increase can be calculated according to the linear temperature coefficient of resistance α (see (1)) with respect to the resistance of the wire at room temperature [19, 22]. To determine α we measured the temperature dependence of gold nanowires similar to the nanowires that are utilized in the electromigration measurements in the range of 4.2 K $< T <$ 300 K by applying low currents (up to approximately 1 μA) to avoid Joule heating of the wires. From these measurements, $\alpha = 0.002\ \mathrm{K}^{-1}$ was determined for a temperature of 273 K according to:

$$\alpha = \frac{\delta R_{\mathrm{th}}}{\Delta T R_0}. \tag{1}$$

The question that arises is how the (relative) resistance increase depends upon the applied current density. Figure 1 displays the resulting dependence of the relative resistance change, $\Delta R/R_0$, and the corresponding temperature increase as calculated from (1), both as a function of the different current densities applied to a gold nanowire. The experiment is conducted as follows: the current is applied in steps of 5 mA for a time interval of 5 min, followed by a cooling period without any current. At the beginning of each current step the resistance change, and thus the temperature increase due to Joule heating, is calculated. Typically, a relative resistance increase of about 15% generates a temperature increase of about 80 K.

The black line in figure 1 shows the best fit to the resistance data using $y = Ax^m$ as a fit function. It is known from the literature that the temperature increase due to Joule heating

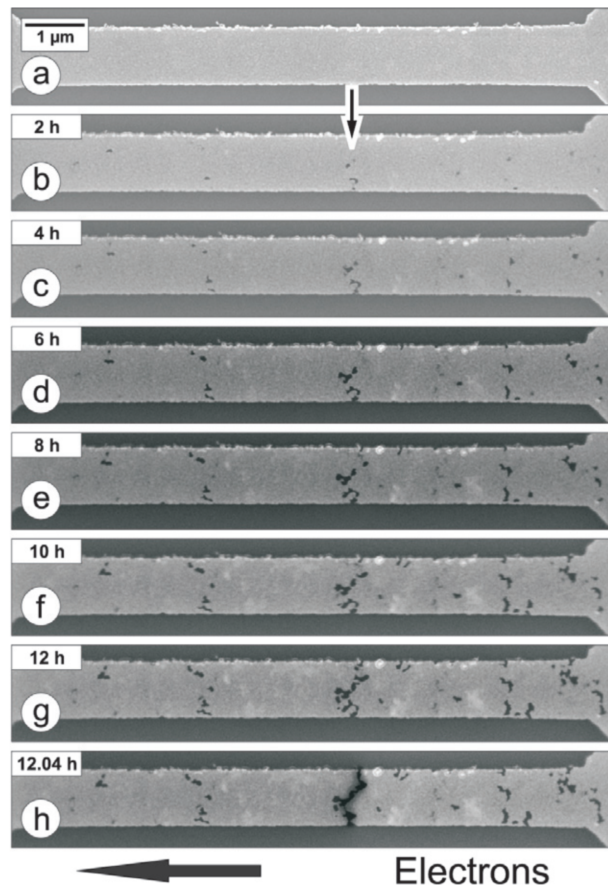

Figure 2. Morphological development of a polycrystalline gold nanowire. Image (a) shows the wire before any voltage is applied. Images (b)–(g) are acquired in a 2 h interval with electrons flowing from right to left. Image (h) shows the wire after electrical breakdown at a time of 12.04 h. The black arrow indicates the position of electrical breakdown.

can be described as [11] $\Delta T \sim R_{\text{th}} \cdot P = R_{\text{th}} \cdot R(I, T) \cdot I^2$. Since the resistance R_{th} also depends on the temperature increase due to Joule heating, the temperature increase can be written as $\Delta T = A \cdot I^m$, with A being a material constant depending on the geometry and heat conductivity of the materials involved and m being a 'thermal' current exponent.

Since the temperature increase is directly coupled to the relative resistance increase, the exponent m from figure 1 may be called a 'thermal' current exponent which describes the dependence of the relative resistance increase (which is proportional to the temperature increase) to an applied current density for polycrystalline gold nanowires on silicon substrates. Using the fit function, the value $m = 2.32$ can be used to calculate the *expected* temperature increase due to the increasing current density. This will be important in the discussion given in section 3.4.

3.2. Morphological developments

In figure 2 the development of voids and hillocks of a typical fine-grained gold nanowire is shown chronologically. Image (a) is acquired before any voltage is applied to the wire. The

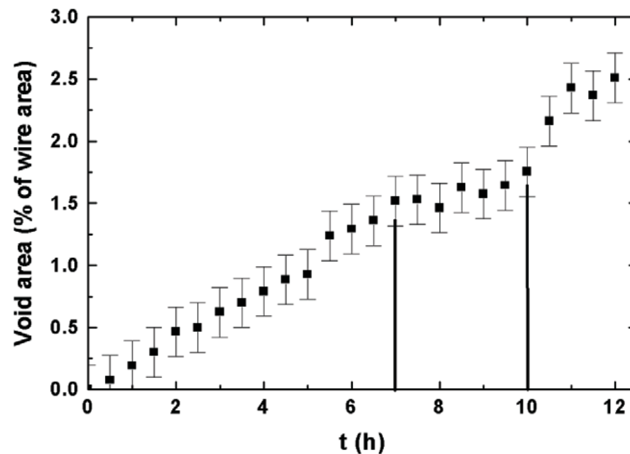

Figure 3. Area of the voids visible in figure 2 with respect to the area of the whole nanowire. A linear increase in the void area during the experiment is obvious without an incubation time at the beginning of current flow. An estimated error of 0.2% due to the measurement procedure is considered by the error bars.

images (b)–(g) are acquired after 2 h time intervals between each image. A two-point voltage of 1.5 V is applied, leading to a current of approximately 40 mA (i.e. the current density has a value of $j \simeq 1.2 \times 10^8$ A cm^{-2} at the beginning of the experiment); image (h) is acquired directly after electrical breakdown of the wire at a time of 12.04 h.

The black arrow between figures 2(a) and (b) indicates the position of the first voids (dark contrast), which developed in this experiment. This is also the breakdown position of the wire (see figure 2(h)). The critical voids develop in a slit-like manner perpendicular to the current direction. Besides, undercritical voids are formed on both sides of the breakdown position, which also develop perpendicular to the wire axis. In contrast to the critical voids, these undercrititcal voids do not develop further, as one can see from figures 2(e)–(h). These uncritical voids could also develop into critical voids, provided that there are no other critical voids. The development into a critical void is associated with an enhanced local temperature (see section 3.4) and, in turn, to a higher diffusivity, which leads to faster migration at this point. As expected for a metallic nanowire, where the wind force dominates over the direct force [23, 24], we find a tendency for void nucleation and growth at the cathode side, which leads predominantly to an accumulation of hillocks between the position of the critical voids and the cathode. The hill-like species are formed by the migrated gold atoms, which coalesce with nearby gold grains. According to the SEM images, the growth direction is perpendicular to the plane of the nanowire. After the gold wire is broken, the mean thickness—as controlled by AFM measurements—remained constant, except the sites where hillocks are created. However, due to the small lateral dimension of the hillocks, this has a minor effect on the total resistance (see section 3.3).

We would like to mention that a controlled observation of the development of the critical voids is only possible using the constant-voltage mode. Using this mode, melting near the position of the critical voids is prevented.

To investigate the morphological development of the nanowire further, the void area with respect to the area of the whole nanowire is determined from SEM images, as shown in figure 2 for a 30 min time interval. As given in figure 3, we find a linear increase in the void area up to $t = 7$ h, followed by a region (7 h $\leqslant t \leqslant$ 12 h) where the void area remains almost constant, as

one can recognize from looking at figures 2(e), (f). After 10 h of electrical stressing, the void area increases more rapidly before the nanowire finally fails.

It is interesting to mention that, even in these fine-grained, polycrystalline wires where the grain boundaries are the main diffusion pathways [25], the total sum of the void area increases linear in time. Such a linear increase in void area has been measured in bamboo-like aluminium wires for single voids [13]. Please note that, in our experiment, the total area of the voids is considered. The arising question is whether a linear growth of void area is trivial or if it has a deeper physical meaning.

Kraft showed in his PhD Thesis [26] that the number of voids for a polycrystalline wire is proportional to the width of the wire and the current density. In this work he also modelled the development (growth and shape changes) of a *single* void under the assumption of a linear growth of void area. The description of the modelled development of the shape of a single void under electromigration fits very well to the experimental results as presented in [26]. Moreover, theoretical calculations by Sanchez *et al* [12] showed that, for voids of different shapes, the void volume increases linearly in time under the assumption of a locally constant mass flux.

It is important to note that, for these considerations, the void volume is the crucial parameter. Since we find columnar grain growth for our gold wires, we can also take the void area as the crucial parameter, which is an assumption that is also applied in some theoretical works [27].

As discussed above, for only *single* voids a linear increase in the void area is found to be typical, which is mainly based on the assumption that the mass flux is constant in time. In contrast, in our experiments we have to consider that *many* voids of different shapes (and positions in the nanowire) generate different mass fluxes. Moreover, the mass can flow into already existing voids which would lead to a decrease in the void area.

Looking in more detail into the morphological changes of the nanowire displayed in figure 2, we do not find regions where voids are shrinking or even vanishing. Instead, we observe that voids are still growing. Since we also observe that hillocks on top of the nanowire grow, it is rather likely that the mass flow remains constant, which in turn explains the linear increase in the total void area.

Surprisingly, we find that the void area remains constant for the time interval 7 h $\leqslant t \leqslant$ 10 h. From this and following the preceding arguments, we can conclude that no mass flow exists (see figure 3). Since mass flow is directly connected to diffusion processes, we have to answer the question of which diffusion mechanism is responsible for the strong decrease in the mass flow. We can exclude that volume diffusion is effective due to the high activation energy [3] compared to the other diffusion mechanisms. That is, grain boundary and surface diffusion are the dominant processes in the present nanowires. To explain our data, we assume that, after 7 h of electrical stressing, grain boundary diffusion becomes inactive due to relaxation processes within the grain boundaries. This is correlated to the reduction of the number of diffusion channels, so that surface diffusion becomes the dominant mechanism. Since the number and size of voids remains constant (see figures 2(e), (f)), the mass flow seems to be extremely low. However, this does not mean that surface diffusion also becomes inactive. It is possible that the wind force generates a mass flow predominantly from or to the hillocks which is not detectable due to carbon contaminations occurring in the SEM.

After a time interval of $\Delta t \simeq 3$ h, which may be related to a so-called incubation time [13], the void area (see figure 3) increases at an even higher rate compared to the beginning of the electromigration process. As one can see from figures 2(g), (h), this occurs specifically in the vicinity of the critical voids.

To study the behaviour described above in more detail, we determine the current density at the position of the critical voids. Figure 4 shows the current density as a function of time in

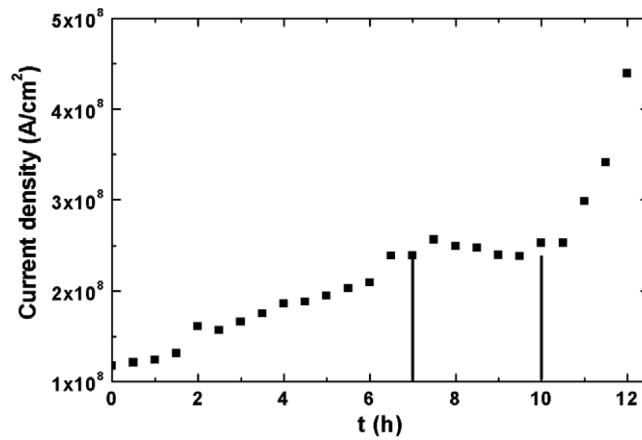

Figure 4. Development of the current density at the position of the critical voids. After a linear increase for about 7 h, the current density saturates for an interval of 3 h. After 10 h of electrical stressing, a sharp increase in the current density occurs, followed by the electrical breakdown of the wire at this position (see figure 1(f)).

30 min steps, as obtained from the corresponding SEM images with respect to the measured current I.[2] A linear increase in the local current density is observed for the time interval $0\ \text{h} \leqslant t \leqslant 7\ \text{h}$. In this time interval the local current density increases from a value of $j_{\text{loc},0\ \text{h}} \simeq 1.2 \times 10^8\ \text{A cm}^{-2}$ to a value of $j_{\text{loc},7\ \text{h}} \simeq 2.5 \times 10^8\ \text{A cm}^{-2}$. This indicates that, at the position of the critical voids, the width of the wire decreases linearly with time. For the time interval $7\ \text{h} \leqslant t \leqslant 10\ \text{h}$, the current density remains constant. This is also the time interval where the void area remains constant (see figure 3 and also figures 2(e), (f)). After about 10 h the current density begins to increase drastically until the wire finally fails after 12.04 h at a current density of $j_{\text{loc}} \simeq 4.4 \times 10^8\ \text{A cm}^{-2}$.

The breakdown of the wire finally occurs in a slit-like manner at the position of the highest current density (see figure 2(f)) with a gap of approximately 10 nm. Failure in a slit-like manner has been observed previously for polycrystalline, near-bamboo and single-crystalline aluminium wires [17, 25, 28, 29]. In the case of the bamboo and single-crystalline wires, failure occurs often in a transgranular manner, indicating that stress migration might play a dominant role [30]. Our fine-grained polycrystalline gold wires have no passivation layer, which might enhance the build up of mechanical stress. Therefore, electromigration and voiding takes place in the grain boundaries and at triple points and stress migration should not play a dominant role in the failure process. That in our polycrystalline wires the failure is due to slit-like voids might be explained by a resistor network. If, in such a network, a resistor fails, the other resistors in the vicinity are subjected to a higher load and therefore the possibility that they also fail is enhanced. This leads to the propagation of a line of broken resistors (which represents a slit-like void) perpendicular to the applied current. Such behaviour has already been studied theoretically by Wu *et al* [31] and Pennetta *et al* [18]. They simulated the electromigration failure in a polycrystalline wire within a biased percolation model and found a similar damage pattern, as is observed in our experiments, i.e. the formation of a (one-dimensional) slit-like void perpendicular to the current direction leading to electrical breakdown.

[2] A minor part of the current might flow through the substrate or through carbon contaminations. After electrical breakdown, a residual current of 0.9 mA remains, but this is only 2.8% of the current directly before breakdown. Therefore, we have neglected this current in the calculations.

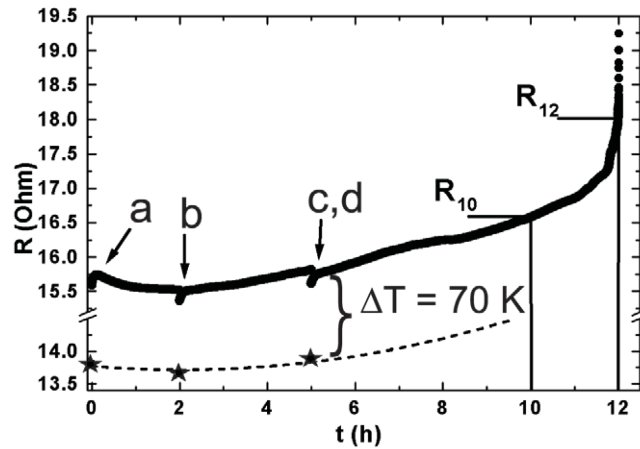

Figure 5. Resistance behaviour of the wire shown in figure 2. At the beginning of each part of the electrical stressing (marked with (a), (b) and ((c), (d)); see arrows) a sharp increase in the resistance is observed. The overall development of the resistance shows a slight decrease for the first 2 h, followed by a constant increase up to about 11 h. In the last hour of electrical stressing the resistance increases sharply until finally the wire fails.

3.3. Resistance behaviour

In this section the resistance as a function of time will be discussed with respect to the morphological developments as already shown in figures 2–4.

Figure 5 shows the resistance R as a function of time for the nanowire shown in figure 2. The full line displays the resistance data during the electrical stressing of the nanowire. The stars indicate the resistance before the electromigration experiment had started (figure 2(a)) and whenever the experiment was interrupted (figures 2(b)–(d)). The jump-like resistance increase at the beginning (a) and after 2 h (b) and 5 h ((c), (d)), respectively, is due to Joule heating when the voltage is applied (see also section 3.1). A temperature increase of about $\Delta T = 70$ K is calculated from (1) according to a resistance change of $\Delta R = 1.85\ \Omega$ (see figure 5(a)).

When the voltage is applied for the first time (figure 5(a)) and after thermalization of the nanowire, the resistance decreases slightly in the first 2 h of the experiment by about 0.075 Ω. This is most likely due to relaxation processes taking place due to the high current flow [32]. After 2 h the resistance starts to increase linearly at a rate of $3 \times 10^{-5}\ \Omega\ \mathrm{s}^{-1}$, which yields a resistance increase of about 1 Ω within 8 h. As mentioned above, the resistance of the nanowire taken at room temperature (stars) is about $\Delta R = 1.85\ \Omega$ lower compared to the *in situ* measurements. It is interesting to note that ΔR is almost constant at the positions marked (a), (b), and (c) in figure 5. Furthermore, the difference ΔR can be extrapolated up to $t = 10$ h. This means that the temperature increase during electrical stressing remains constant. This behaviour is indicated by the dashed line in figure 5, which nearly parallels the *in situ* resistance data. As we have shown recently [19], this indicates that morphological changes dominate the resistance behaviour up to $t = 10$ h.

After about 10 h, the resistance starts to increase drastically according to the development of the critical voids at the breakdown position. This behaviour is directly correlated to the local current density (see figure 4). Whether this resistance increase is due to morphological or due to temperature effects will be discussed in the next section.

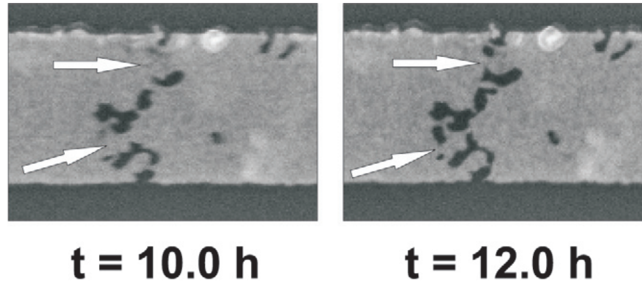

Figure 6. Morphological development at the position of the critical voids after 10.0 and 12.0 h, respectively. The development and coalescence of the voids within this time interval is recognizable. The white arrows mark the positions of the gold area which is taken into account for the resistance and temperature calculations.

3.4. Detailed analysis of breakdown position

As discussed above, we interpret the resistance increase between the beginning of the experiment and $t = 10$ h as being mainly dominated by morphological changes, whereas the temperature of the nanowire remains almost constant. After $t = 10$ h the resistance increases rapidly, which is reflected by a strong increase in the local current density at the position of the critical voids from $j_{10} = 2.5$ A cm^{-2} to a value of $j_{12} = 4.4$ A cm^{-2} for $t = 12$ h. The question arises of whether the strong resistance increase before the breakdown is dominated morphologically or by an increase of the local temperature in the vicinity of the critical voids.

Figure 6 shows details of the morphological development of the critical voids displayed in figure 2 at times of 10.0 and 12.0 h, respectively. The white arrows indicate the main remaining pathways of the gold nanowire which are responsible for the conductivity.

At the beginning of the experiment the nanowire exhibits a resistance of $R = 13.8\ \Omega$ while having the following dimensions: thickness $t = 36$ nm, length $l = 9600$ nm and width $w = 960$ nm. Thus, the resistivity has a value of $\rho \simeq 5\ \mu\Omega$ cm.

Using the local resistivity we can calculate the resistance of the nanowire close to the position of the critical voids. Taking into account the shape (length and width) and number of voids, the local resistance of the remaining gold pathways at the critical voids are calculated to be $\delta R_m(10\ \text{h}) = 0.46\ \Omega$ and $\delta R_m(12\ \text{h}) = 1.09\ \Omega$, respectively.

Additionally, we have to consider that, besides the resistance increase caused by morphological changes δR_m, a temperature-induced resistance increase δR_{th} also has to be taken into account. Thus, the resistance of the wire under investigation can be written as follows:

$$R_t = R_0 + \Delta R_w + \delta R_m(t) + \delta R_{th}(t) \tag{2}$$

where R_0 is the resistance of the thermalized wire at the beginning of the experiment and ΔR_w is the resistance increase due to morphological changes within the nanowire—apart from the critical void area.

As discussed above, we can assume that, up to $t = 10$ h, mainly morphological changes are responsible for the resistance increase, i.e. we assume that $\delta R_{th}(10) \simeq 0$. Furthermore, looking at the morphological development of the gold wire for $t > 10$ h, we find (see figure 2) that mainly the void area of the critical voids changes rapidly, whereas the void area of the other parts of the wire remain almost constant; i.e. $R_w \simeq$ const. Under these conditions the

difference in the increases in resistance at $t = 12$ and 10 h can be written as:

$$R_{12} - R_{10} = \delta R_m(12\text{ h}) + \delta R_{th}(12\text{ h}) - \delta R_m(10\text{ h}). \quad (3)$$

Since we find, from figure 5, a value of $R_{12} - R_{10} = 1.4\ \Omega$, we can calculate $\delta R_{th}(12\text{ h})$ from (3) using the data for δR_m as given above, which yields a value of $\delta R_{th}(12\text{ h}) = 0.77\ \Omega$. According to (1) this allows us to calculate the local temperature increase at the breakdown position, which is $\Delta T_{loc} = 350$ K for $t = 12$ h.

This value of the temperature enhancement is surprisingly low when taking the current densities into account. At a time of $t = 12$ h the local current density has a value of $j_{12} = 4.4 \times 10^8$ A cm^{-2}. Using the data in figure 1, this should lead to a resistance increase of $\delta R_{th}(t = 12\text{ h}) = 3.1\ \Omega$, which would lead to a temperature increase of about $\Delta T_{12} = 1400$ K. The same considerations at a time of $t = 10$ h with a current density of $j_{10} = 2.5 \times 10^8$ A cm^{-2} lead to a resistance increase of $\delta R_{th}(t = 10\text{ h}) = 0.35\ \Omega$ and a temperature increase of $\Delta T_{10} = 350$ K.

These values, which are calculated according to the current density, might be overestimated for the following reasons: due to the higher temperature gradient at the breakdown position, the local temperature will be lower, as expected. Furthermore, the resistivity ρ might be reduced due to annealing effects, e.g. a reduction of point defects, which would lead to a reduced Joule heating. The reduction of point defects could also be a reason for higher values of the temperature coefficient of resistance, α, which in turn lowers the expected temperature increase according to (1). Scorzoni *et al* (see [11] and references therein) have shown that a deviation in α appears due to electromigration-induced changes in the grain structure, which yields a value of $\Delta\alpha \simeq 0.1\%$.

Taking these considerations into account, the local temperature increase of the order of 1400 K, as derived from the high current density, seems not to be realistic. Instead, our analysis of the resistance data, together with the *in situ* observation of the morphological changes, clearly shows that the local temperature increase in the vicinity of the critical voids is of the order of $\Delta T \simeq 350$ K. This observation is quite important for simulations of the temperature distribution in electromigration experiments, since the local temperature increase calculated simply by geometrical considerations and Joule heating ($\delta R_{th} \sim A \times j^m$ with $m = 2$, as it is applied in some theoretical work [18, 33]) seems to be highly overestimated. A more accurate calculation is presented in [34], but it is unclear if $m = 2$ is used for the calculations. To prove the statements given above, microscopic measurements of the temperature profile of a nanowire have to be carried out. This may be possible by using a thermo-atomic force microscope, which possesses a resolution of about 50 nm [35].

4. Conclusion

In this paper we investigated the morphological development of fine-grained gold nanowires under electromigration. Failure of the nanowires under investigation takes place through classical void growth and through failure due to the formation of slit-like voids in the final stages. The void area in the nanowires increases linearly with time, indicating an overall constant mass flux in the first part of the experiment. From the resistance data taken *in situ* during the electromigration experiment, we can distinguish between morphological and temperature-induced effects and are able to determine quantitatively the temperature-induced resistance increase in the time region where the breakdown of the nanowire starts. The current density was found to increase by a factor of four at the position of the breakdown. But this increase in current density most likely does not lead to a major temperature increase, i.e. no hot spot is formed until for the very last stages of the experiment.

Acknowledgments

This work was supported by the Deutsche Forschungsgemeinschaft under the programme 'Sonderforschungsbereich 616: Energy Dissipation at Surfaces'. Valuable discussions with J Krug, A Ney and D Sudfeld are acknowledged.

References

[1] Pierce D G and Brusius P G 1997 *Microelectron. Reliab.* **37** 1053
[2] Blech I A and Meieran E S 1967 *Appl. Phys. Lett.* **11** 263
[3] Ho P S and Kwok T 1989 *Rep. Prog. Phys.* **52** 301
[4] Tu K N 2003 *J. Appl. Phys.* **94** 5451
[5] Hau-Riege C S and Thompson C V 2001 *Appl. Phys. Lett.* **78** 3451
[6] Hau-Riege C S 2004 *Microelectron. Reliab.* **44** 195
[7] Black J R 1969 *IEEE Trans. Electron. Devices* **16** 338
[8] Lee K L, Hu C K and Tu K N 1995 *J. Appl. Phys.* **78** 4428
[9] Cho J and Thompson C V 1989 *Appl. Phys. Lett.* **54** 2577
[10] Christou A 1994 *Electromigration and Electronic Device Degradation* (New York: Wiley)
[11] Scorzoni A, Neri B, Caprile C and Fantini F 1991 *Mater. Sci. Rep.* **7** 143
[12] Sanchez J E Jr, McKnelly L T and Morris J W Jr 1990 *J. Electron. Mater.* **19** 1213
[13] Arzt E, Kraft O, Nix W D and Sanchez J E Jr 1994 *J. Appl. Phys.* **76** 1563
[14] Suo Z, Wang W and Yang M 1994 *Appl. Phys. Lett.* **64** 1944
[15] Schimschak M and Krug J 2000 *J. Appl. Phys.* **87** 695
[16] Boularot H and Bradley R M 1996 *J. Appl. Phys.* **80** 756
[17] Yoo Y-C and Thompson C V 1997 *J. Appl. Phys.* **81** 6062
[18] Pennetta C, Alfinito E, Reggiani L, Fantini F, DeMunari I and Scorzoni A 2005 *Phys. Rev.* B **70** 174305
[19] Stahlmecke B and Dumpich G 2005 *Defect Diffus. Forum* **237–240** 1163
[20] Stahlmecke B and Dumpich G 2007 in preparation
[21] Stahlmecke B and Dumpich G 2007 *Appl. Phys. Lett.* at press
[22] EIA/JESD33-A 1995 *Standard Method for Measuring and Using the Temperature Coefficient of Resistance to Determine the Temperature of a Metallization Line* Electronic Industries Assoziation, Engineering Department p 15
[23] Stahlmecke B, Meyer zu Heringdorf F-J, Chelaru L, Horn von Hoegen M, Dumpich G and Roos K R 2006 *Appl. Phys. Lett.* **88** 053122
[24] Gupta R P 1982 *Phys. Rev.* B **25** 5188
[25] Cho J and Thompson C V 1990 *J. Electron. Mater.* **19** 1207
[26] Kraft O 1995 *PhD Thesis* University Stuttgart
[27] Trattles J T, O'Neill A G and Mecrow B C 1994 *J. Appl. Phys.* **75** 7799
[28] Sanchez J E Jr, McKnelly L T and Morris J W Jr 1992 *J. Appl. Phys.* **72** 3201
[29] Marieb T, Flinn P, Bravman J C, Gardner D and Madden M 1995 *J. Appl. Phys.* **78** 1026
[30] Kirchheim R 1992 *Acta Metall. Mater.* **40** 309
[31] Wu K and Bradley R M 1994 *Phys. Rev.* B **50** 12468
[32] Rost M J, Quist D A and Frenken J W M 2003 *Phys. Rev. Lett.* **91** 026101
[33] Sasagawa K, Naito K, Kimura H, Saka M and Abè H 2000 *J. Appl. Phys.* **87** 2785
[34] Kraft O and Arzt E 1995 *Appl. Phys. Lett.* **66** 2063
[35] Meckenstock R and Spoddig D 2006 private communication